Inverse wavefield extrapolation revisited: limitations of single- and multi-valued operators

C.P.A Wapenaar and J.T. Fokkema, Centre for Technical Geoscience, Delft University of Technology;*
J.W. Thorbecke, Silicon Graphics

Summary

Most approaches to inverse wavefield extrapolation have in common that the operator is defined as the time-reversed (or complex conjugated) forward operator. Despite the time-symmetry of the wave equation, this time-reversal introduces errors even for the simple situation of a homogeneous medium and an infinite aperture. In strongly inhomogeneous media the kinematical aspects of multi-valued events are handled correctly, but angle-dependent errors occur in their dynamical behaviour.

Introduction

Inverse wavefield extrapolation plays a central role in seismic migration. Independent of the actual numerical implementation, most approaches have in common that the inverse extrapolation operator is defined as the time-reversed or, in the frequency domain, complex conjugated forward operator. This stems from the simple fact that the acoustic wave equation is symmetrical in time. In this paper we analyze the limitations of inverse extrapolation with time-reversed forward operators.

The infinite aperture paradox

It is well known that wavefield extrapolation of data recorded on a *finite* aperture is not exact. The extrapolated wavefield contains artefacts that can be kinematically explained as ghost wavefields radiated by secondary sources located at the endpoints of the aperture, see Figure 1. Suppose now that the data would be recorded on an infinite aperture. Then *forward* wavefield extrapolation would be exact: the ghost wavefield of the secondary sources at the 'endpoints' would vanish when these endpoints were moved towards infinity, see Figure 2a. Since the wave equation is symmetrical in time, one would expect a similar conclusion for *inverse* extrapolation from an infinite aperture. However, it will appear that the artefacts do not vanish in this case, see Figure 2b. First we show this with a numerical experiment. Consider the configuration in Figure 3. A monopole point source (0 to 60 Hz) is situated at $z_s = 400$ m below the center of a circular aperture with radius $\rho_{\max}$; the propagation velocity is $c = 1200$ m/s. The response of this point source

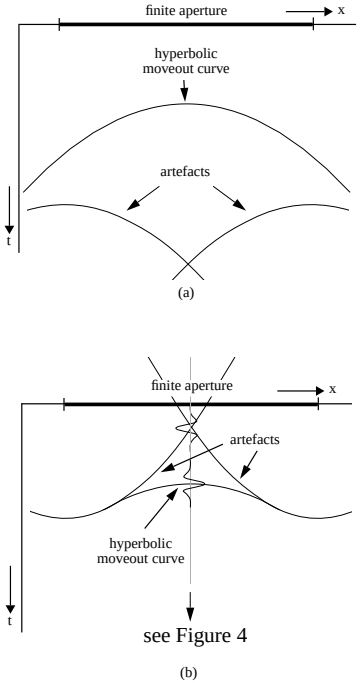

Fig. 1: *'Results' of forward (a) and inverse (b) wavefield extrapolation of a point source response recorded on a finite aperture. Note that both results contain artefacts as a result of the finite aperture.*

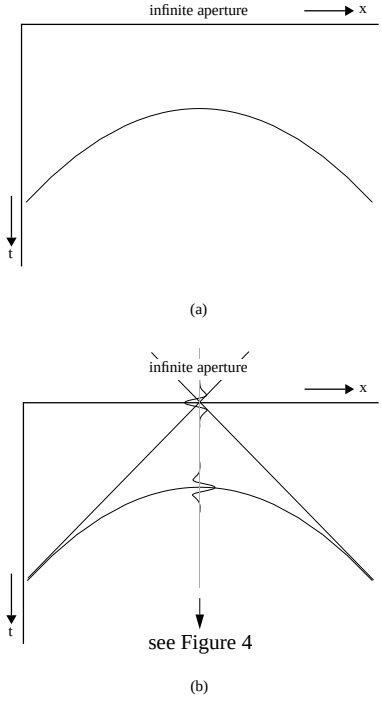

Fig. 2: *'Results' of forward (a) and inverse (b) wavefield extrapolation of a point source response recorded on an infinite aperture. The inverse extrapolation result contains artefacts, despite the infinite aperture.*

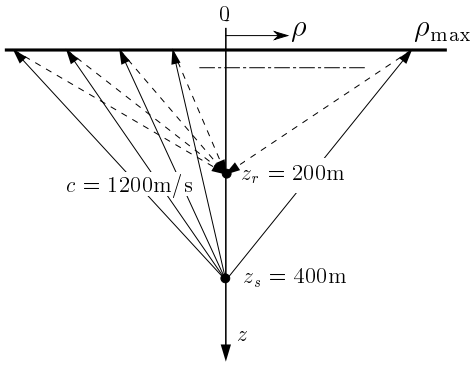

Fig. 3: *The response at the surface of the source at $z_s = 400$ m will be inversely extrapolated to the indicated point at $z_r = 200$ m.*

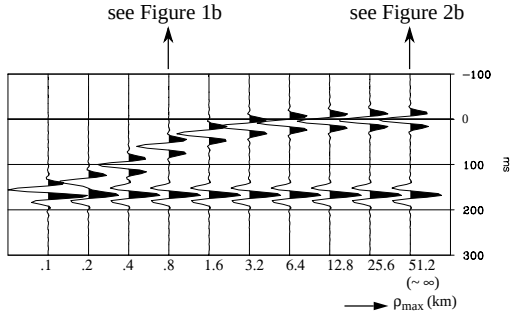

Fig. 4: *Inverse extrapolation result at the indicated point ($z_r = 200$ m) in Figure 3 for increasing values of the aperture radius. Note the persistent artefact at $t = 0$.*

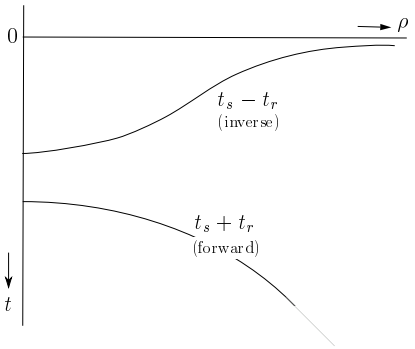

Fig. 5: *Traveltime curves in forward and inverse extrapolation. The stationary behaviour of $t_s - t_r$ for $\rho \to \infty$ explains the artefacts in Figures 2b and 4.*

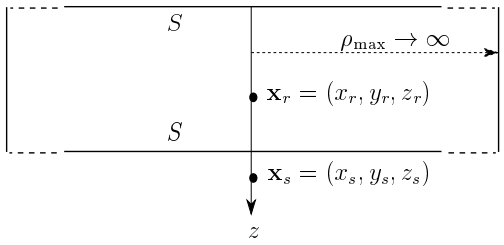

Fig. 6: *The evaluation of the integral in equation (2) along the closed surface S yields the exact wavefield at $\mathbf{x}_r$.*

is inversely extrapolated to a point at $z_r = 200$ m below the center of the aperture. Figure 4 shows the result for increasing values of the aperture radius $\rho_{\max}$. Apart from the expected event at $t = (z_s - z_r)/c = 166$ ms we observe an artefact with opposite sign that gradually moves towards $t = 0$ as $\rho_{\max}$ approaches infinity. To understand what causes this artefact, consider the curve $t_s - t_r$ in Figure 5, where $t_s = \sqrt{z_s^2 + \rho^2}/c$ and $t_r = \sqrt{z_r^2 + \rho^2}/c$ represent the traveltimes of the point source response and the operator, respectively (see Figure 3). In the inverse extrapolation procedure, events along the traveltime curve $t_s - t_r$ are integrated. The stationary behaviour of this curve for $\rho \to \infty$ is responsible for the artefact at $t = 0$ in Figure 4 for $\rho_{\max} \to \infty$. For an analytical justification, see [9]. Since the curve $t_s + t_r$ does not become stationary for $\rho \to \infty$, forward extrapolation to a point above the aperture does not yield this artefact.

Another way to explain this fundamental difference between forward and inverse wavefield extrapolation is based on an analyis of the representation integral [5, 11, 3]

$$P(\mathbf{x}_r, \omega) = \oint_S [G\nabla P - P\nabla G] \cdot \mathbf{n} \mathrm{d}S. \qquad (1)$$

Here S is a closed integration surface with outward pointing normal vector $\mathbf{n}$, P is the acoustic wavefield in the space-frequency $(\mathbf{x}, \omega)$ domain related to sources outside S and G is the forward propagating (or causal) Green's wavefield of a point source at $\mathbf{x}_r$ inside S. Exploiting the time symmetry of the wave equation we may also write

$$P(\mathbf{x}_r, \omega) = \oint_S [G^* \nabla P - P\nabla G^*] \cdot \mathbf{n} \mathrm{d}S, \qquad (2)$$

where G^* (the complex conjugate of G) is a backward propagating (or anti-causal) Green's wavefield. Representation (1) is the basis for forward and (2) for inverse wavefield extrapolation; both representations are exact. The reason why inverse wavefield extrapolation yields artefacts, despite the exactness of representation (2), is because in this representation the closed surface cannot be replaced by an infinite planar surface without approximation. Figure 6 shows the appropriate closed surface for the configuration considered above (Figure 3). The contribution of the integral in equation (2) over the side surface vanishes when $\rho_{\max} \to \infty$. However, analyzing the contribution of the integral over the lower surface (between $\mathbf{x}_r$ and $\mathbf{x}_s$) learns that the two terms $G^* \nabla P \cdot \mathbf{n}$ and $-P\nabla G^* \cdot \mathbf{n}$ cancel, except for the evanescent wavefield [11]. Hence, integrating only along the up-

per surface (as in Figure 3) is equivalent to ignoring evanescent waves. This is in agreement with Berkhout and van Wulfften Palthe [1], who derived inverse wavefield extrapolation as a spatial deconvolution process that ignores evanescent waves.

In conclusion, the artefacts of inverse wavefield extrapolation from an infinite aperture can be explained as non-vanishing 'endpoint' contributions or as erroneously handled evanescent waves.

Limitations of multi-valued operators

Recently the effect of multi-valued traveltimes on migration and inversion has received a lot of attention [4, 8, 6, 2, 7]. In this section we apply a similar analysis as above to inverse wavefield extrapolation with time-reversed multi-valued operators.

Consider the configuration in Figure 7, which contains a synclinal structure that gives rise to triplications. Figure 8 shows the response at the surface of a dipole source at $z_s = 1400$ m, vertically below the center of the aperture. For the inverse extrapolation from the surface to the indicated point at $z_r = 1200$ m we use an operator based on the Green's wavefield related to a monopole source at this point. Figure 9 shows this Green's wavefield (convolved with a wavelet to get a better display). Applying the time reversed version of this operator to the data in Figure 8, i.e., cross-correlating Figures 8 and 9 trace by trace, one would expect *quintuples* appearing in the result. On the other hand, from the configuration in Figure 7 we would expect that the inverse extrapolation result at z_r is single valued, because the medium between z_r and z_s is homogeneous.

Figure 10 shows the trace by trace cross-correlation. Note that this result indeed contains quintuple events. The extrapolation result at the indicated point at z_r in Figure 7 is obtained by adding these traces, see Figure 11a. The main contribution comes from the stationary event at $t = (z_s - z_r)/c = 66$ ms in Figure 10; the other contributions of the quintuples cancel and the endpoint contributions are much weaker than in our 'infinite aperture' example (dipole instead of monopole source; 2-D instead of 3-D configuration). For comparison, Figure 11b contains the direct modeled result, scaled to the same maximum amplitude; Figure 12 shows the inverse extrapolation result for all points at $z_r = 1200$ m. From this numerical example it is clear why we obtain a single event at the correct travel time.

Next, for the amplitude analysis, we consider again the representation (2). Also for inhomogeneous media this representation yields the exact wavefield at $\mathbf{x}_r$, provided the integral is taken over a closed surface S. Figure 13 shows the appropriate closed surface for the considered configuration. The contribution of the integral in equation (2) over the side surface vanishes again when $\rho_{\max} \to \infty$. From Figure 13 we observe that the contribution from the lower integration surface (the dashed line between $\mathbf{x}_r$ and $\mathbf{x}_s$) contains, amongst others, the correlation of the *scattered* wavefield and the *scattered* Green's function. Since both these wavefields are single valued (in this example), their correlation is also single valued. Figure 14 shows the result of the integral along the lower surface for all $\mathbf{x}_r$ with $z_r = 1200$ m. Note that this result should be added to that of Figure 12 in order to obtain the full wavefield at $z_r = 1200$ m. The first event in Figure 14 is the single-valued correlation result we just discussed. It occurs at the same time as the inverse extrapolation result in Figure 12; its amplitude is proportional to $R^2(\alpha)$, where $R(\alpha)$ is the angle-dependent reflection coefficient of the synclinal interface. The

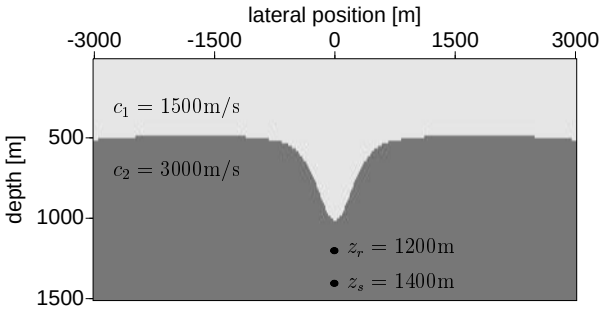

Fig. 7: *The response at the surface of the source at $z_s = 1400$ m will be inversely extrapolated to the indicated point at $z_r = 1200$ m.*

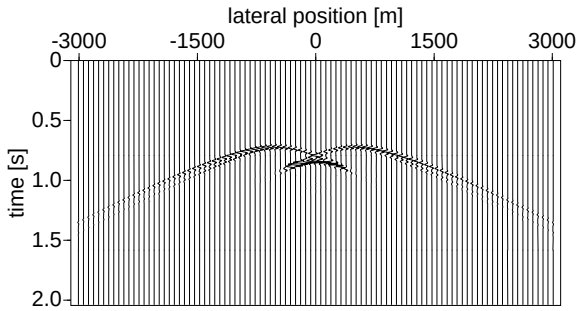

Fig. 8: *The response at the surface of the source at $z_s = 1400$ m. Note the triplications. (Modeled with finite differences).*

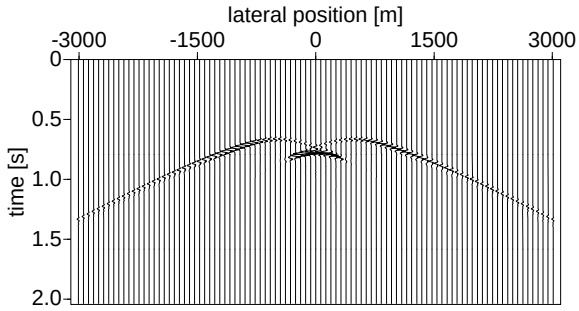

Fig. 9: *The Green's wavefield at the surface (convolved with a wavelet), due to the Green's source at $z_r = 1200$ m. (Modeled with finite diff.).*

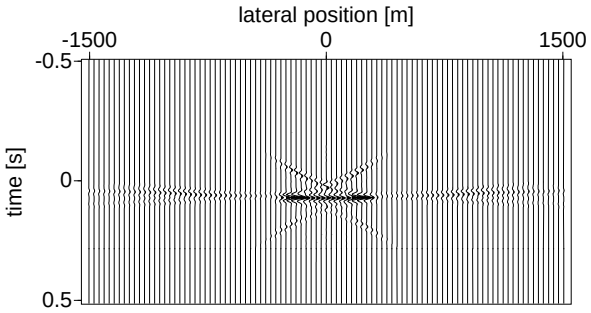

Fig. 10: *The trace by trace cross-correlation of Figures 8 and 9. Note the quintuple events.*

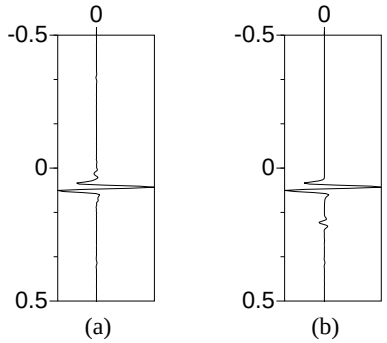

Fig. 11: *(a) Sum of the traces of Figure 10. This is the inverse extrapolation result at the indicated point at $z_r = 1200$ m. (b) For comparison, direct modeled response.*

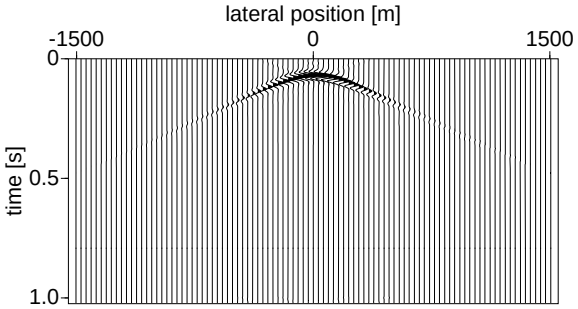

Fig. 12: *Inverse extrapolation result at all points at $z_r = 1200$ m.*

second event in Figure 14 is the reflected downgoing wavefield at $z_r = 1200$ m.

From this analysis we may conclude that the inverse extrapolation result in Figure 12 represents the upgoing wavefield only and that it contains an angle-dependent amplitude error.

Conclusion and discussion

Despite the time-symmetry of the acoustic wave equation, inverse wavefield extrapolation with time-reversed (or complex conjugated) operators is not exact, even for the simple situation

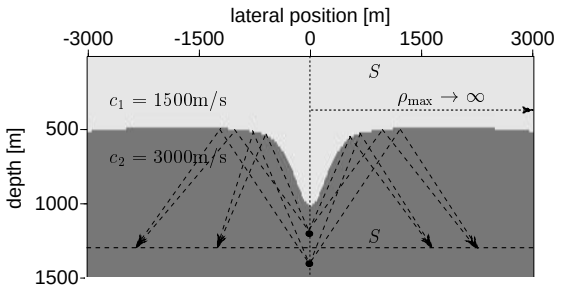

Fig. 13: *The contribution of the integral (2) over the lower surface (the dashed line) is ignored in the inverse extrapolation result of Figure 12.*

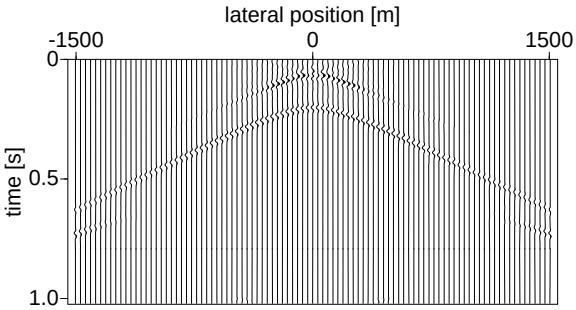

Fig. 14: *Contribution of the integral along the dashed line in Figure 13 for all points at $z_r = 1200$ m.*

of a homogeneous medium and an infinite aperture.

In strongly inhomogeneous media the kinematical aspects of multi-valued events are handled correctly, but angle-dependent errors occur in their dynamical behaviour. In [11, 10] we propose improved operators that correct for these errors. Using reciprocity, the required modifications can be derived from the cross-correlation of the seismic reflection measurements.

References

[1] A. J. Berkhout and D. W. van Wulfften Palthe. Migration in terms of spatial deconvolution. *Geophys. Prosp.*, 27(1):261–291, 1979.

[2] A. Ehinger, P. Lailly, and K. J. Marfurt. Green's function implementation of common-offset, wave equation migration. *Geoph.*, 61:1813–1821, 1996.

[3] J. T. Fokkema and P. M. van den Berg. *Seismic applications of acoustic reciprocity*. Elsevier, Amsterdam, 1993.

[4] S. Geoltrain and J. Brac. Can we image complex structures with first-arrival traveltime? *Geoph.*, 58:564–575, 1993.

[5] P. M. Morse and H. Feshbach. *Methods of theoretical physics, Vol. I.* McGraw-Hill Book Company Inc., New York, 1953.

[6] C. J. Nolan and W. W. Symes. Imaging and coherency in complex structures. In *Soc. Expl. Geophys., Expanded Abstracts*, pages 359–362, 1996.

[7] A. P. E. ten Kroode and D. J. Smit. A microlocal analysis of migration. In *Inverse problems in geophysical applicatons.* SIAM, Philadelphia, 1997.

[8] W. J. F. Van Geloven and G. C. Herman. Crosswell tomography using generalized traveltime inversion. In *Soc. Expl. Geophys.*, pages 446–449, 1995.

[9] C. P. A. Wapenaar. The infinite aperture paradox. *J. Seismic Expl.*, 1:325–336, 1992.

[10] C. P. A. Wapenaar. One-way representations of seismic data. *Geoph. J. Int.*, 127:178–188, 1996.

[11] C. P. A. Wapenaar and A. J. Berkhout. *Elastic wave field extrapolation.* Elsevier Amsterdam, 1989.